

# A Method for Determining the Envelope of Induced Electric Field on a Simple Human Head Model by Peaks Detection

Mario Cvetković, *Member, IEEE*, Hrvoje Dodig, *Member, IEEE*, and Dragan Poljak, *Senior Member, IEEE*

Original scientific article

**Abstract**—This paper is on the use of a hybrid boundary element method/finite element method (BEM/FEM) to determine the induced electric field in spherical human head models exposed to high-frequency plane electromagnetic (EM) wave. The geometrically simplified models include the homogeneous one and the non-homogeneous one, featuring compartments such as skin, skull, CSF, and brain. Both models are illuminated by plane EM wave at frequencies including 900 and 1800 MHz, 3500 MHz pertaining to 5G communication systems and also 6000 MHz representing the transition frequency related to the EMF safety standards. The numerical results for the electric field induced in both human head models are presented, while the emphasis is on the electric field along the propagation axis. The novelty of this work is related to the subsequent post-processing of the sampled induced field along the model axis by using two different numerical filtering techniques. It is shown that using the peak detection algorithm, the spline interpolation could be used to estimate the signal envelope. The exponentially decaying nature of the envelope allows to assess the penetration depth of the EM radiation within the biological tissue. Moreover, it is shown that the analytically calculated penetration depth, derived for the unbounded medium, is well reproduced by the numerical computation of EM field.

**Index Terms**—Computational dosimetry, human exposure to EMF, hybrid BEM/FEM, high-frequency dosimetry, numerical filtering.

## I. INTRODUCTION

The assessment of human exposure to high-frequency (HF) electromagnetic fields (EMF) requires the use of computational dosimetry models since experimental procedures are often difficult to implement [1]. There are many computational methods utilised to facilitate this, but also to aid in the development of exposure standards related to human safety due to EMF exposure [2]. The latest documents related to human EMF exposure include the revised IEEE standard from 2019 [3] and the ICNIRP guidelines from 2020 [4], respectively, specifying the exposure limits in terms of basic restrictions serving as a substitute for the temperature increase

in the HF range. These documents specify the dosimetric quantity in terms of the specific absorption rate (SAR) at frequencies below 6 GHz (considered transition frequency) and the absorbed power density (APD) above 6 GHz. Both SAR and APD are calculated in the post-processing stage from the output of electromagnetic dosimetry model, i.e. the induced electric field. The resulting temperature rise [5], [6] in the exposed human body can be determined using the subsequent thermal dosimetry model using the calculated SAR or APD as inputs [7], [8].

One important and well known characteristic of the electromagnetic wave exposure in the HF range is the low penetration depth, inversely proportional to the frequency of the EM wave. In the GHz range, the penetration of EM wave is limited to superficial layers. For example, in the case of the mm-waves from the higher frequency spectrum of the latest generation (5G) of wireless communication systems, the penetration depth is limited to skin tissue, resulting in the use of a simplified planar skin models such as one-dimensional stratified models [9], [10], or stratified block models [11], [12]. It should be noted that the ongoing work of the standards organisations such as the IEEE International Committee on Electromagnetic Safety (ICES) is currently focused on extending the dosimetric models to spherical and cylindrical geometries [11].

Compared to geometrically simple dosimetry models, the use of anatomically precise geometrical models of the human body or body parts [13] is limited in the high-frequency range, due to low penetration depth but also due to computational requirements. This is especially difficult when the computational method is based on the integral equation approach such as surface integral equation (SIE) [14]. From the computational resources point of view, the main limit of SIE is related to the discretisation of HF problem, resulting in a large fully populated system matrix. The excessive time requirements of numerical full-wave techniques is recognised even when considering the accuracy of telecommunication channel modeling [15]. However, the restriction on the matrix size could be somewhat curtailed by employing the hybrid method such as boundary element method/finite element method (BEM/FEM), which has previously been used in the human exposure HF assessment [8]. This work is on the use of a hybrid BEM/FEM to determine the induced electric field in the several human head models irradiated by high-frequency EMF. The subsequent post-processing of the numerical results is carried out

Manuscript received January 16, 2024; revised February 9, 2024. Date of publication March 5, 2024. Date of current version March 5, 2024. The associate editor prof. Giovanna Calò has been coordinating the review of this manuscript and approved it for publication

M. Cvetković and D. Poljak are with the Faculty of Electrical Engineering, Mechanical Engineering and Naval Architecture, University of Split, Split, Croatia (corresponding author: mcvetkov@fesb.hr).

H. Dodig is with Faculty of Maritime Studies, University of Split, Split, Croatia.

Digital Object Identifier (DOI): 10.24138/jcomss-2023-0180

to correlate with the exponentially decaying field and the analytically calculated penetration depth. The first step is to test whether numerical filtering techniques, such as the moving root mean square or the peak detection approach could be utilised to this end. If it can be shown on the anatomically simple models, it is conceivable to be useful even in the case of the geometrically complicated models, thus alleviating some computational burden when HF dosimetry problems are considered.

This work should be considered an extension of authors approach used in [16] by additional post-processing and analysis of the induced electric field results by applying two numerical filtering techniques. The main contribution of the paper is in the use of a spline interpolation algorithm to estimate the envelope of the induced electric field in the canonical human head geometry. Also, it is demonstrated that the peak detection approach is not suitable to this end. In addition to transverse-magnetic (TM) polarization [16], transverse-electric (TE) polarization has been considered in this work, as well as post-processing using the proposed approach of the induced electric field obtained at several additional frequencies.

The organisation of the paper is as follows: following the introductory part, mathematical background related to the utilised EM computational dosimetry model is given as well as its verification. Also, brief description of the used human head models is given. The numerical results for the induced electric field is presented in the next section. Moreover, the results of the subsequent post-processing at several frequencies is given in order to correlate with the penetration depth at the particular frequency. The concluding remarks are given in the final section, while derivation of the analytical expression for penetration depth is given in the Appendix.

## II. MATHEMATICAL BACKGROUND

### A. Electromagnetic Dosimetry Model

The human head exposed to incident electromagnetic radiation can be treated as a classical scattering problem. In case of a time-harmonic field, the problem can be specified using the following integro-differential expressions. The exterior domain is treated by the Stratton-Chu integral equation facilitating the rephrasing of both electric and magnetic fields in terms of their tangential components [17]:

$$\alpha \vec{E}'_{ext} = \vec{E}'_{inc} + \oint_{\partial V} \hat{n} \times (\nabla \times \vec{E}_{ext}) G dS + \oint_{\partial V} [(\hat{n} \times \vec{E}_{ext}) \times \nabla G + (\hat{n} \cdot \vec{E}_{ext}) \nabla G] dS \quad (1)$$

where  $\hat{n}$  represents the normal on the problem boundary  $\partial V$  (between interior and exterior region),  $V$  is domain of the problem while  $\alpha$  is the solid angle subtended at the observation point. The total electric field and the incident electric field are denoted by  $\vec{E}_{ext}$  and  $\vec{E}'_{inc}$ , respectively, while  $G$  represents the free space Green's function:

$$G = G(\vec{r}, \vec{r}') = \frac{e^{-jkR}}{4\pi R}; \quad R = |\vec{r} - \vec{r}'| \quad (2)$$

where  $R$  is the distance from the observation point to the source point,  $\vec{r}$  and  $\vec{r}'$ , respectively, and  $k$  is the wave number.

The interior domain of the problem (human head) is governed by the following equation [17]:

$$\nabla \times \left( \frac{j}{\omega \mu} \nabla \times \vec{E}_{int} \right) - (\sigma + j\omega \epsilon) \vec{E}_{int} = 0 \quad (3)$$

where  $int$  denotes the interior domain, while  $\epsilon$ ,  $\sigma$ ,  $\mu$  are the parameters of the inhomogeneous domain, namely electric permittivity, conductivity, and magnetic permeability, respectively. Finally,  $\omega = 2\pi f$  denotes the angular frequency.

The expressions (1) and (3) can be coupled and numerically solved using a hybrid BEM/FEM method. The interested reader could find details on the applied BEM/FEM procedure in [8], [17].

### B. EM Model Verification

Verification of the utilised EM model based on the hybrid BEM/FEM approach has been performed using the geometry of the metallic slab covered by two different dielectrics, illuminated by plane EM wave, as depicted on the inset of Fig. 1. The calculation of the bistatic RCS has been carried out in both E plane and H plane, respectively. The results were compared with the results obtained by hybrid VSIE formulation [18] and also with the well known commercial software FEKO, based on the traditional conformal MoM/FEM formulation. The results for the bistatic RCS in E plane, given in Fig. 1a), show very good agreement between the hybrid BEM/FEM and other two approaches. Similarly very good agreement between hybrid BEM/FEM and FEKO is obtained for the bistatic RCS in H plane, as depicted in Fig. 1b), while the results for the hybrid VSIE formulation are offset by 0.5-0.8 dB.

It should be noted that the additional extensive verification of the hybrid BEM/FEM model used in this work has been carried out in [17].

### C. Spherical Head Models

The numerical results for the induced electric field in the human head, presented in the following section, are obtained using the two spherical head models. The first model (non-homogeneous) consists of four compartments (tissues), including the outer head layer (modeled as the skin), the boneous skull, the cerebrospinal fluid (CSF), and the brain, while the second model is a homogeneous one, with the same dimensions, as depicted in Fig. 2a).

The frequency dependent electrical properties of the model, namely, the conductivity  $\sigma$  and the relative permittivity  $\epsilon_r$  are given in Table I. The values for a dry skin tissue are used as parameters of the homogeneous head model. All parameters were taken from study by Gabriel [19].

It should be noted that meshes of both homogeneous and non-homogeneous models are identical, the only difference being in the tissues properties assigned to specific finite element used to discretise the head. This will enable the subsequent comparison using the thermal dosimetry models, not reported in this work.

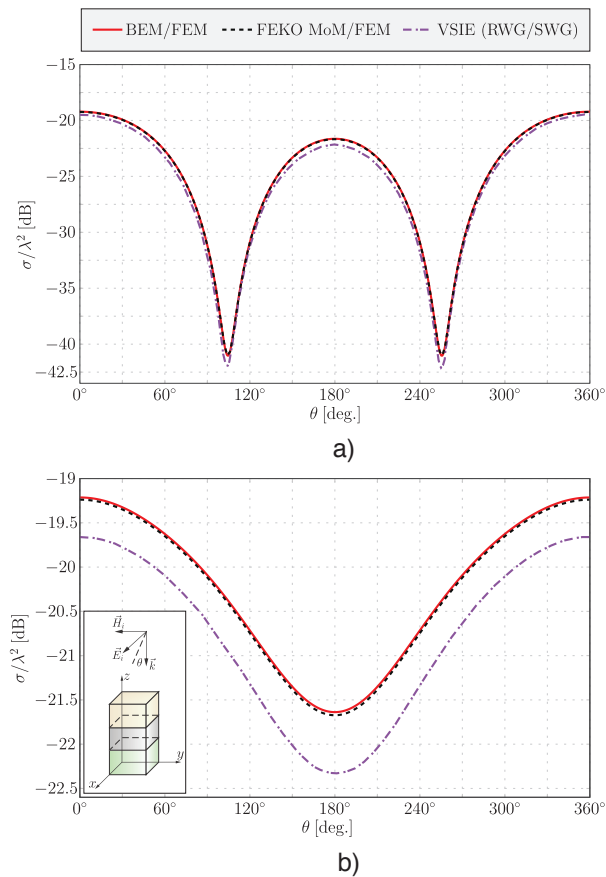


Fig. 1. Bistatic RCS in: a) E plane and b) H plane for metallic slab covered with two different dielectrics. Comparison with commercial software FEKO (MoM/FEM) and VSIE (RWG/SWG) by [18]

TABLE I  
HOMOGENEOUS MODEL FREQUENCY DEPENDENT PARAMETERS (DRY SKIN TISSUE VALUES): CONDUCTIVITY  $\sigma$ , RELATIVE PERMITTIVITY  $\epsilon_r$ , WAVELENGTH  $\lambda$  AND PENETRATION DEPTH  $\delta$  [16].

$f$ [GHz]	$\sigma$ [S/m]	$\epsilon_r$	$\lambda$ [mm]	$\delta$ [mm]
0.9	0.86674	41.405	50.714	40.23
1.8	1.1847	38.872	26.416	28.252
3.5	2.0249	37.005	13.946	16.102
6.0	3.8912	34.946	8.34	8.1734
10.0	8.0138	31.29	5.2291	3.7979
30.0	27.099	15.51	2.2937	0.85351
60.0	36.397	7.9753	1.5245	0.47805
90.0	38.989	5.9364	1.1878	0.38183

The human head model is discretised using 12.251.851 tetrahedral finite elements, while the head is enclosed in the surrounding box of air (representing the domain boundary) whose surface (related to BEM) is meshed using 7.472 triangular elements. The finite element mesh of the head model interior is depicted in Fig. 2b).

The Intel Pardiso direct solver was used to solve the resulting sparse matrix system. It took around 20 hours of computational time to complete the filling of the system matrix and solving it.

#### D. The Penetration Depth

The penetration depth (or skin depth)  $\delta$  represents the distance to which an incident electromagnetic wave penetrates

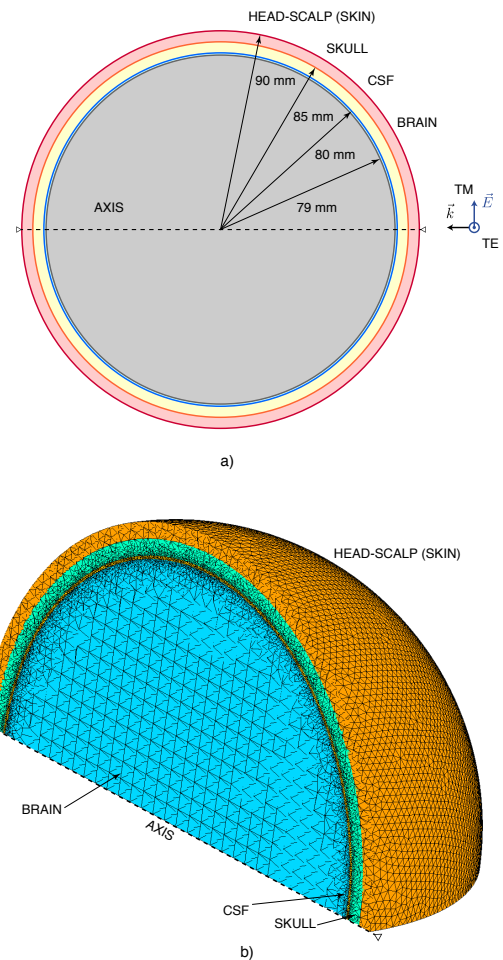


Fig. 2. Simplified human head model: a) non-homogeneous model with corresponding dimensions and the direction of incident electric field (TE and TM polarization), and b) Finite element mesh of the spherical model (only quarter of model depicted). The dotted line (AXIS) depicts the points where electric field is calculated and later post-processed. The electric field is sampled at 2000 points along this axis.

the medium. The skin depth is usually defined as the depth at which the amplitude of the plane wave electric field or magnetic field in a homogeneous unbounded half-space decreases to a factor  $1/e$  of its surface value, assuming maximum amplitude  $E_0$  at the surface, as illustrated in Fig. 3.

The above definition of the skin depth is usually associated with the plane wave propagating in the unbounded medium [20], [21], however, the concept of plane wave skin depth is also applied to study the effective skin depth due to large circular loop and horizontal electric dipole sources [22]. Even in cases such as large source-receiver distances and/or high frequencies and half-space conductivities, the effective skin depth tends to the plane wave skin depth.

The penetration depth  $\delta$  for the homogeneous isotropic dielectric medium with losses can be calculated using the following expression:

$$\delta = \frac{c}{\omega \sqrt{\frac{\epsilon_r}{2} \left[ \sqrt{1 + \frac{\sigma^2}{\omega^2 \epsilon_0^2 \epsilon_r^2}} - 1 \right]}} \quad (4)$$

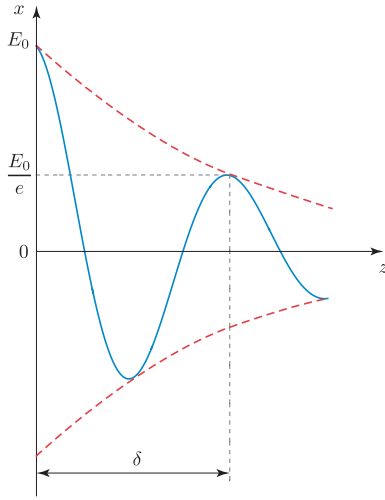


Fig. 3. Illustration of skin depth and the associated envelope of a signal (dashed line) [16].

where  $c$  is the wave velocity in free space, and  $\varepsilon_0$  is the permittivity of free space. The derivation of the expression (4) can be found in the Appendix.

The values of penetration depth at several frequencies of interest are given in Table I. As evident from Table I, the penetration depth at 6 GHz corresponds to 8 mm, while at 30 GHz, it is less than 1 mm. This is the reason the term *millimeter-wave* is used in this frequency range.

As evident from Fig. 3, the oscillating amplitude of the signal (the electric field along the propagation axis) can be represented by a smooth exponentially decaying curve that smoothly encloses the signal. This curve is termed the envelope of the signal and is represented by the dashed line in Fig. 3.

The wavelength of the electromagnetic wave propagating in the homogeneous lossy dielectric can be determined using the following expression:

$$\lambda = \frac{\lambda_0}{\sqrt{\frac{\varepsilon_r}{2} \left[ \sqrt{1 + \frac{\sigma^2}{\omega^2 \varepsilon_0^2 \varepsilon_r^2}} + 1 \right]}}; \quad \lambda = \frac{\lambda_0}{\sqrt{\varepsilon_r}} \quad (5)$$

where  $\lambda_0$  is wavelength in free space, and  $\varepsilon_r$  is relative permittivity of the material. The corresponding values of  $\lambda$  are given in Table I, while derivation of (5) can be found in the Appendix.

### III. NUMERICAL RESULTS

The EM dosimetry model based on hybrid BEM/FEM, introduced in the last section, was used to obtain the numerical results presented in this one. The plane EM wave with  $S_{eq} = 10 \text{ W/m}^2$  power density is incident on the human head model. The side of the spherical model where EM wave enters the head will be termed anterior side, as later on we will focus on the results along the propagation axis (from the anterior side). The following frequencies of the EM wave are considered: 900 MHz, 1800 MHz, 3500 MHz and 6000 MHz.

The last two correspond to operating frequency of 5G systems in Croatia (3.4 - 3.6 GHz), and to the transition frequency (6 GHz) from the safety standards [8], respectively. The results are presented in Figs. 4-12.

#### A. Electric Field Induced in Human Head

The first set of results, presented in Figs. 4-5, depict the induced electric field distribution in two spherical models.

Two polarizations of incident plane wave have been considered, transversal magnetic (TM), shown in Fig. 4, and the transversal electric (TE), shown in Fig. 5. The comparison of induced electric field in the transversal cross-sections of both homogeneous and non-homogeneous models shows different distributions between the two polarizations, however, very similar distribution is obtained when considering two models at the particular polarization. The highest value of the induced electric field is obtained near the model surface (skin layer), although this is more difficult to discern at two higher frequencies (3.5 GHz and 6 GHz). Also, the results for both models clearly illustrate the lower penetration depth with the increasing frequency.

Since the curvature of the sphere is uniform, this geometry minimises the influence of geometrical features such as folds, bumps and other irregularities - present in the detailed anatomical models - on the electric field distributions. Also, due to model symmetry, the values of the induced electric field along the horizontal axis will be identical for both polarizations, hence, we can neglect the wave polarization in the following, and thus focus on the middle of the model (axis).

The distribution of the induced electric field along the axis of propagation (anterior side on the left) is shown in Fig. 6. Compared to Figs. 4-5, Fig. 6 more clearly depicts the lower penetration depth when frequency is increased. The wavelike behaviour of the signal (induced electric field) can be seen in Fig. 6, as well as the exponential decay with the increasing frequency. The non-exponential distribution in the middle regions at two lower frequencies is due to the presence of standing waves.

#### B. Specific Absorption Rate

Additionally, the specific absorption rate (SAR) can be calculated using the well-known relation:

$$\text{SAR} = \frac{\sigma}{2\rho} |E|^2 \quad (6)$$

where  $E$  denotes the peak value of the induced electric field at the point of interest, while  $\rho$  and  $\sigma$  represent the tissue density (in  $\text{kg/m}^3$ ) and the tissue electrical conductivity (in  $\text{S/m}$ ), respectively. Results for the SAR calculated at the first 500 anterior points along the propagation axis are given in Fig. 7.

The comparison of SAR, given in Fig. 7, between homogeneous and non-homogeneous spherical model indicates the following: at two lower frequencies, the non-exponential decay is evident in non-homogeneous model. Also, the discontinuity of SAR at tissue interfaces is in accordance with [9]. The explanation is straightforward: as the boundary conditions

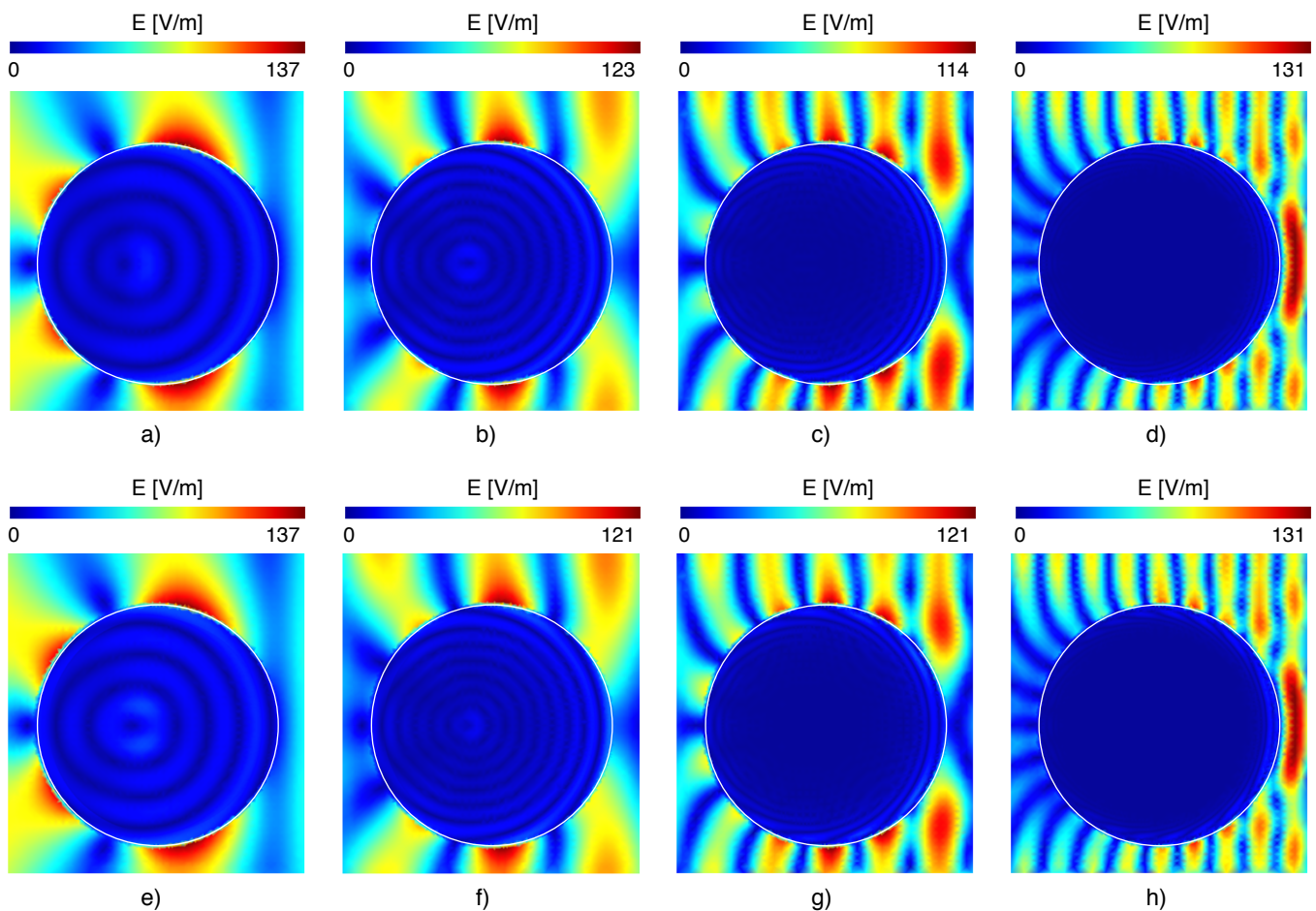


Fig. 4. Comparison of the electric field distribution in the spherical model and the surrounding region. Cross-section of homogeneous sphere: a) – d), and non-homogeneous sphere: e)–h), at frequencies of interest. TM polarization of the wave [16].

prescribe that the tangential component of electric field is continuous across the tissue interface, and the orientation of electric field is parallel to this interface for both polarizations, the SAR will be proportional to the tissue conductivity.

It should also be noted that as the frequency increases, the exponential decay of the induced electric field, and hence, SAR, becomes more pronounced. More importantly, the difference between the homogeneous and non-homogeneous distributions becomes less evident. As the same trend is expected to continue at even higher frequencies, we can now introduce the skin depth  $\delta$  for the homogeneous medium calculated using (4), as shown in Fig. 7.

### C. Proposed Method of Signal Envelope Detection

The following includes numerical filtering of the results presented in Fig. 6, in order to detect the envelope of the electric field (signal). Two different techniques are utilised to post-process the input signal, the first approach being the moving root mean square (RMS) and other the peak detection algorithm.

1) *Moving RMS*: The expression for the moving RMS of the signal, denoted by  $X_{RMS}$ , is given by [16]:

$$X_{RMS}(t) = \sqrt{\frac{1}{T} \int_{t-T}^t x^2(\tau) d\tau} \quad (7)$$

where moving operation can be taken at any reference  $t$ , thus behaving like a filter.

The calculation of discrete form of (7) is carried out using [16]:

$$X_{RMS}[i] = \sqrt{\frac{1}{N} \sum_{k=1-N+1}^i x^2[k]} \quad (8)$$

where  $x[k]$  is signal sample, and  $N$  is the sliding window size.

Using the RMS approach, a window of specified length is moved over the data samples and the RMS is computed over the data in the window.

Figs. 8-11 depict the envelope of electric field distribution (signal) using various sizes of window length  $N$ . The results are shown only at the first 500 anterior points of spherical models. As evident from Figs. 8-11, the smooth exponentially decaying shape of the signal is not possible to obtain using the RMS approach, regardless of the window size. The failure of RMS approach to capture the smooth nature of exponential curve, has lead us to use another approach, based on peak detection.

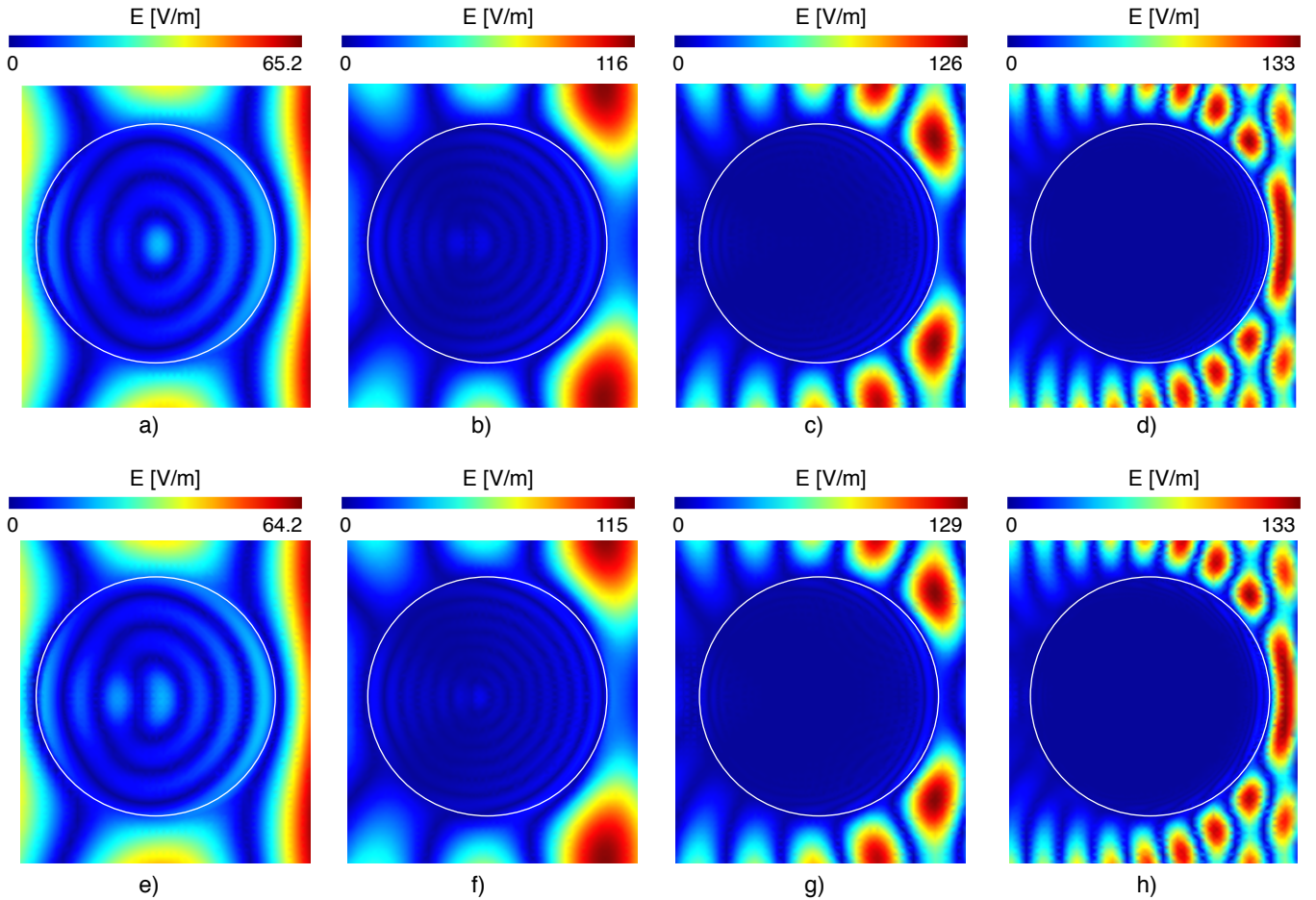


Fig. 5. Comparison of the electric field distribution in the spherical model and the surrounding region. Cross-section of homogeneous sphere: a) – d), and non-homogeneous sphere: e)–h), at frequencies of interest. TE polarization of the wave.

2) *Peak Detection*: There are many definitions of signal envelope, including analytic envelope, based on the Hilbert transform. However, in many engineering problems, the envelope detection is not based on analytic signals, and most methods for envelope reconstruction are based on peak detection. In case of amplitude-modulated signals, this is followed by a low-pass filter, usually employing a RC network, to remove the carrier and provide smoothing [23]. The real signal envelopes can be thus obtained from the extrema sampling on signals [24].

The first step in envelope reconstruction is thus to capture the extrema points, as depicted in Fig. 6. The maximum separation  $N$  between local extrema has been determined by a trial and error procedure, taking into account the particular frequency (i.e. wavelength), as given in Table II.

Table II also shows the average separation between the extrema points (maxima) in both homogeneous and non-homogeneous models. More details on the maxima separation can be found in Table III.

Using the detected maxima points, the envelope of the signal (along propagation axis) can be reconstructed using a piecewise cubic spline interpolation, as shown in Fig. 6. More detailed view of the reconstructed envelopes in the anterior regions of spherical head models can be found in Fig. 12.

Fig. 12 shows the results for frequency range 1.8 GHz–6 GHz, while results for 900 MHz are omitted since it was not possible to obtain the exponentially decaying envelope shape. As seen from Fig. 12, depending on the distance between local extrema separations (peak  $N$ ), it is possible to reconstruct the upper (peak) envelope of the signal that follows an exponential decay.

Overlaid on the results in Fig. 12 are the analytically calculated skin depth  $\delta$ , but also the decrease factor  $1/e$  of the maximum electric field. Two values are calculated,  $E_s/e$  and  $E_{env}/e$ , denoting the exponential decrease of the surface electric field and the maximum electric field from the reconstructed envelope, respectively. From the knowledge of  $\delta$  and the maximum field value obtained at the superficial part of the model (head surface), the value of induced electric field could thus be estimated in deeper head tissues.

#### IV. CONCLUSION

This paper presented the numerical results for the electric field induced in two spherical human head models, namely homogeneous and nonhomogeneous one, exposed to plane EM wave radiation. The results are obtained using the state-of-the-art hybrid BEM/FEM formulation. The results of the electric field induced along the axis of propagation are post-

TABLE II

PENETRATION DEPTH  $\delta$  AND WAVELENGTH  $\lambda$  AT SEVERAL FREQUENCIES. AVERAGE SEPARATION BETWEEN ALL DETECTED PEAKS ( $\langle S_{hom} \rangle$ ) IN HOMOGENEOUS AND 4-LAYERS MODEL ( $\langle S_{4L} \rangle$ ).  $\langle S_{hom/4L} \rangle_x$ , WHERE  $x = 4, 5, 6$  DENOTES AVERAGING OVER THE FIRST 4, 5, AND 6 DETECTED PEAKS, RESPECTIVELY.

$f$	$\delta$	$\lambda$	$\langle S_{hom} \rangle$	$\langle S_{4L} \rangle$	$\langle S_{hom} \rangle_4$	$\langle S_{4L} \rangle_4$	$\langle S_{hom} \rangle_5$	$\langle S_{4L} \rangle_5$	$\langle S_{hom} \rangle_6$	$\langle S_{4L} \rangle_6$
[GHz]	[mm]	[mm]	[mm]	[mm]	[mm]	[mm]	[mm]	[mm]	[mm]	[mm]
0.9	40.23	50.714	25.41	25.41	22.52	23.85	25.45	24.39	25.64	25.64
1.8	28.252	26.416	14.82	11.86	9.23	13.23	13.75	9.52	10.58	13.75
3.5	16.102	13.946	7.73	7.11	6.59	7.85	7.38	7.36	7.36	7.38
6.0	8.1734	8.34	7.40	7.01	3.92	3.89	4.42	4.21	5.25	5.26

TABLE III

COMPARISON OF INDIVIDUAL PEAK SEPARATION (PEAKS SEP.) AND AVERAGE PEAK SEPARATION (AVG. PEAK. SEP.) IN HOMOGENEOUS AND NON-HOMOGENEOUS MODELS AT: 900, 1800, 3500, AND 6000 MHz.  $\langle \cdot \rangle_x$ , WHERE  $x = 4, 5, 6$  DENOTES AVERAGING OVER THE FIRST 4, 5, AND 6 DETECTED PEAKS, RESPECTIVELY [16].

Frequency	900 MHz		1800 MHz		3500 MHz		6000 MHz		
	Model	Homogen.	Non-homog.	Homogen.	Non-homog.	Homogen.	Non-homog.	Homogen.	Non-homog.
Peaks sep. (mm)		15.57	15.66	13.68	2.25	7.92	8.91	2.25	2.34
		26.55	21.33	12.60	11.43	7.65	6.66	4.41	4.59
		26.55	26.46	15.84	12.60	5.49	5.58	4.41	5.04
$\langle \cdot \rangle_4$		26.73	26.64	10.80	10.62	10.35	5.22	4.50	3.69
$\langle \cdot \rangle_5$		31.86	31.86	15.84	10.71	5.49	10.44	5.40	5.40
$\langle \cdot \rangle_6$		26.55	31.86	10.71	15.93	5.31	5.31	10.44	10.44
		24.03	24.03	16.02	15.84	10.53	5.40	5.40	5.40
				21.15	10.71	5.40	5.31	5.40	10.53
				21.24	15.84	5.40	5.40	15.84	5.40
				15.84	10.71	10.44	10.44	5.40	10.53
				10.89	10.71	5.40	5.40	5.31	5.40
				13.23	13.32	5.40	5.31	5.40	10.62
						16.02	5.40	10.44	5.40
						5.31	15.75	16.02	10.62
						10.44	5.49	10.80	10.53
						10.71	10.53	10.44	5.49
						5.40	5.49	5.40	10.53
						10.44	10.44	5.31	5.40
						5.40	5.40	5.40	10.53
						5.40	5.31	15.84	5.40
						9.18	5.40	9.27	10.53
						7.02	5.40	5.04	9.27
						7.65	9.09	4.23	3.42
							5.85	5.31	4.59
							8.73		4.05

processed in the subsequent step, using two numerical filtering techniques. The approach based on the envelope reconstruction using the detected peak points yielded a smoothly decaying shape of the signal. This facilitates the correlation of the post-processed results with the analytically calculated penetration depth in the biological tissue. The results of this work could be found relevant in the assessment of human exposure to high-frequency EM fields.

## APPENDIX

To derive the penetration depth  $\delta$  and wavelength  $\lambda$ , we first define the complex relative dielectric constant  $\bar{\epsilon}$

$$\bar{\epsilon} = \epsilon_r - j \frac{\sigma}{\omega \epsilon_0} \quad (9)$$

where  $\sigma$ , and  $\epsilon_r$  represent the conductivity and relative permittivity, respectively,  $\epsilon_0$  is permittivity of free space, and  $\omega = 2\pi f$ , where  $f$  is operating frequency.

The governing equation for the electromagnetic field propagating in an unbounded homogeneous and isotropic dielectric medium with losses, free of sources, is the following wave equation:

$$\nabla^2 \vec{E} + k^2 \vec{E} = 0 \quad (10)$$

where

$$k^2 = \omega^2 \epsilon_0 \mu_0 \bar{\epsilon} \quad (11)$$

In case of an electric field polarized in the  $x$ -direction and propagating in the  $z$ -direction, the solution to (10) is in the form:

$$E_x(z, t) = E_0 e^{j\omega t} e^{\pm jkz} \quad (12)$$

where the sinusoidal harmonic time dependence was assumed.

By defining the complex number  $k$ , from (11), by:

$$k = \beta - j\alpha \quad (13)$$

the expression (12) becomes:

$$E_x = E_0 e^{(j\omega t \pm \beta z)} e^{\pm \alpha z} \quad (14)$$

Based on this solution, the wavelength  $\lambda$  can be defined as:

$$\lambda = \frac{2\pi}{\beta} \quad (15)$$

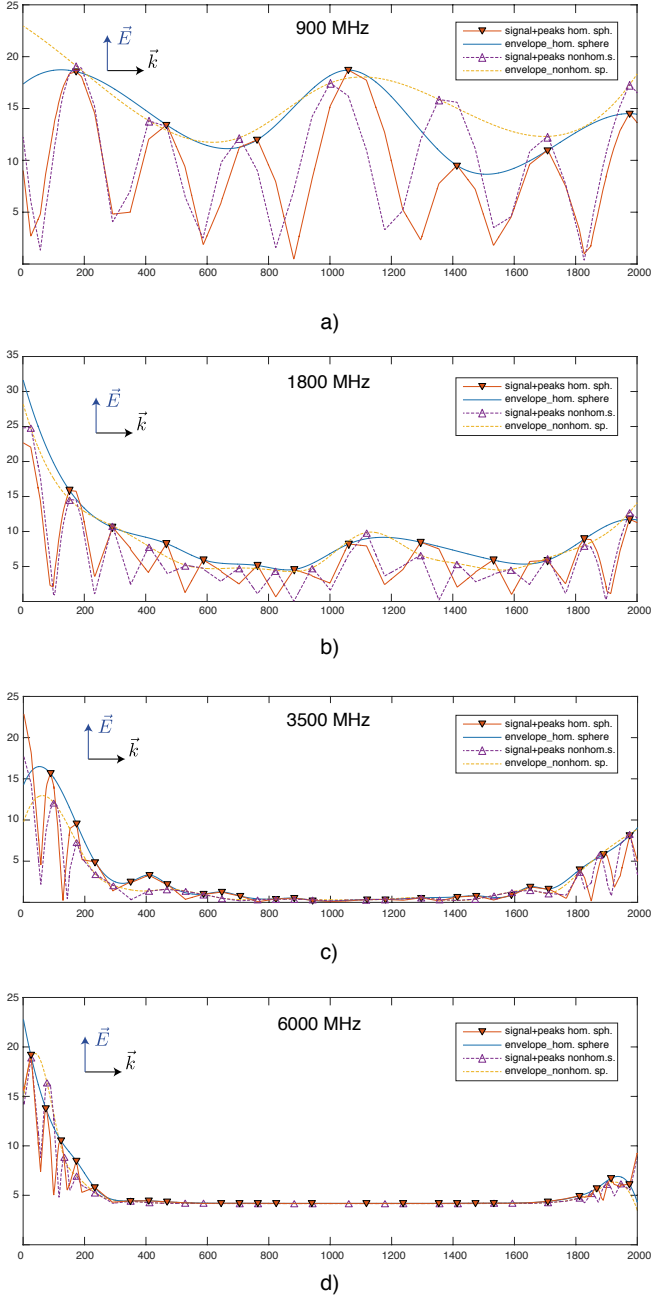


Fig. 6. Numerical filtering of the electric field results along the spherical models' axes. The electric field (signal) at: a) 900 MHz, b) 1800 MHz, c) 3500 MHz, d) 6000 MHz, obtained in the homogeneous model (denoted by hom.) and non-homogeneous (non-hom.) model, respectively. The piecewise cubic spline interpolation of the detected peak points of the signal used to obtain the upper peak envelope. Sample point number (#) denoted on the  $x$ -axis, with  $90 \mu\text{m}$  separation between sampled points. Values of the induced electric field (V/m) on the vertical axis [16].

and the penetration depth  $\delta$  as:

$$\delta = \frac{1}{\alpha} \quad (16)$$

Squaring (13) and using (11) and (9), after some rearranging, we obtain the following system of equations:

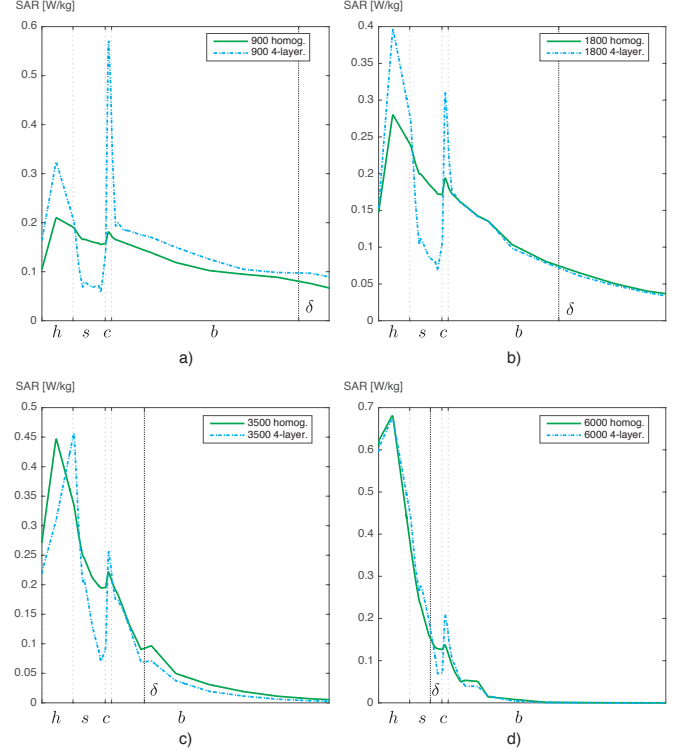


Fig. 7. Comparison of specific absorption rate (SAR) in homogeneous and non-homogeneous (4-layer) models, determined at first 500 points along horizontal axis. Frequency of incident EM wave: a) 900 MHz, b) 1800 MHz, c) 3500 MHz, d) 6000 MHz.

$$\Re(k^2) = \beta^2 - \alpha^2 = \omega^2 \varepsilon_0 \mu_0 \varepsilon_r \quad (17)$$

$$\Im(k^2) = 2\alpha\beta = \omega \mu_0 \sigma$$

Inserting (15) and (16) in (17), the system is transformed into the following:

$$\Re(k^2) = \frac{4\pi^2}{\lambda^2} - \frac{1}{\delta^2} = \omega^2 \varepsilon_0 \mu_0 \varepsilon_r \quad (18)$$

$$\Im(k^2) = \frac{4\pi}{\delta\lambda} = \omega \mu_0 \sigma$$

after some rearranging of (18) we obtain:

$$\frac{16\pi^2}{\delta^2\lambda^2} \left( \frac{4\pi^2}{\lambda^2} - \frac{\omega^2}{c^2} \varepsilon_r \right) = \omega^2 \mu_0^2 \sigma^2 \quad (19)$$

Equation (19) can be written in a canonical form, leading to quadratic equation, whose positive solution is:

$$\frac{1}{\lambda^2} = y = \frac{\pi^2 \omega^2 \varepsilon + \sqrt{\pi^4 \omega^4 \varepsilon^2 + \pi^4 c^4 \omega^2 \mu_0^2 \sigma^2}}{8\pi^4 c^2} \quad (20)$$

After some additional work, we obtain:

$$\frac{1}{\lambda^2} = y = \frac{\omega^2 \varepsilon_r}{8\pi^2 c^2} \left[ 1 + \sqrt{1 + \frac{c^4 \mu_0^2 \sigma^2}{\omega^2 \varepsilon_r^2}} \right] \quad (21)$$

Finally, substituting in (21) the following:

$$c^4 = \frac{1}{\varepsilon_0^2 \mu_0^2} \quad (22)$$

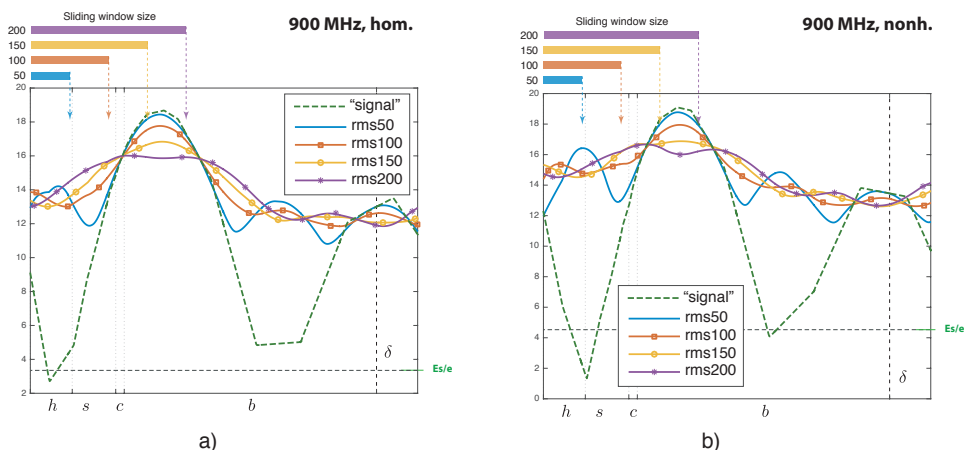


Fig. 8. Incident EM wave frequency  $f=900$  MHz. Envelope of signal (electric field distribution) on the horizontal axis of a) homogeneous and b) non-homogeneous spherical models. Envelope obtained using an RMS approach with sliding window size of 50, 100, 150, and 200 points.  $X$ -axis denotes model tissue (compartment):  $h$  - head,  $s$  - skull,  $c$  - CSF,  $b$  - brain; points separation is  $90 \mu\text{m}$ .  $\delta$  is penetration depth at particular frequency.  $E_s/e$  denotes the 37% value of electric field at the surface.

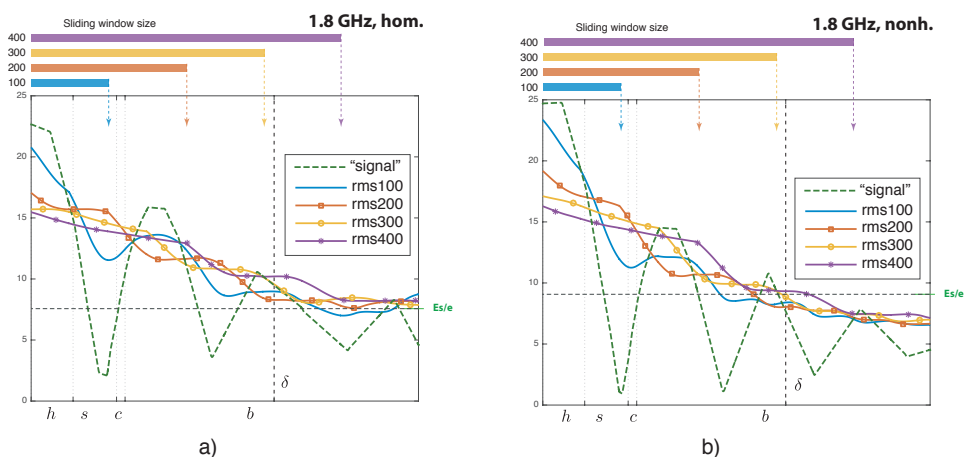


Fig. 9. Incident EM wave frequency  $f=1.8$  GHz. Envelope of signal (electric field distribution) on the horizontal axis of a) homogeneous and b) non-homogeneous spherical models. Envelope obtained using an RMS approach with sliding window size of 100, 200, 300, and 400 points.  $X$ -axis denotes model tissue (compartment):  $h$  - head,  $s$  - skull,  $c$  - CSF,  $b$  - brain; points separation is  $90 \mu\text{m}$ .  $\delta$  is penetration depth at particular frequency.  $E_s/e$  denotes the 37% value of electric field at the surface.

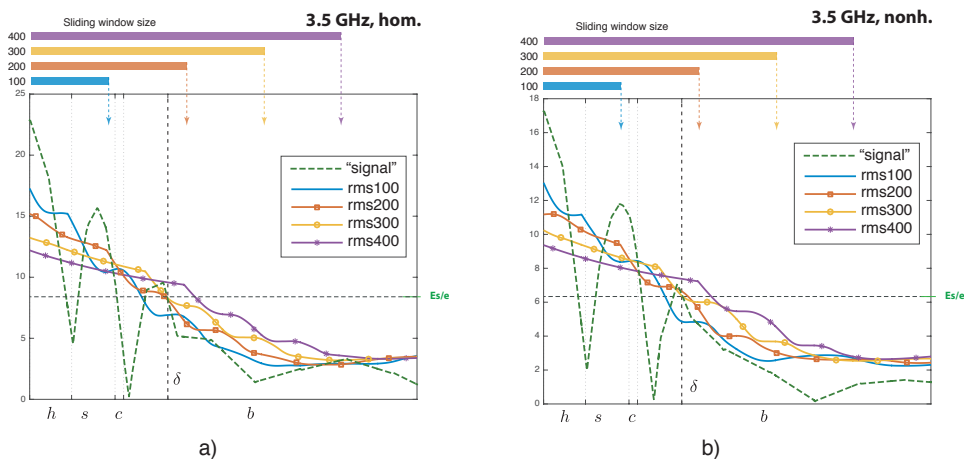


Fig. 10. Incident EM wave frequency  $f=3.5$  GHz. Envelope of signal (electric field distribution) on the horizontal axis of a) homogeneous and b) non-homogeneous spherical models. Envelope obtained using an RMS approach with sliding window size of 100, 200, 300, and 400 points.  $X$ -axis denotes model tissue (compartment):  $h$  - head,  $s$  - skull,  $c$  - CSF,  $b$  - brain; points separation is  $90 \mu\text{m}$ .  $\delta$  is penetration depth at particular frequency.  $E_s/e$  denotes the 37% value of electric field at the surface.

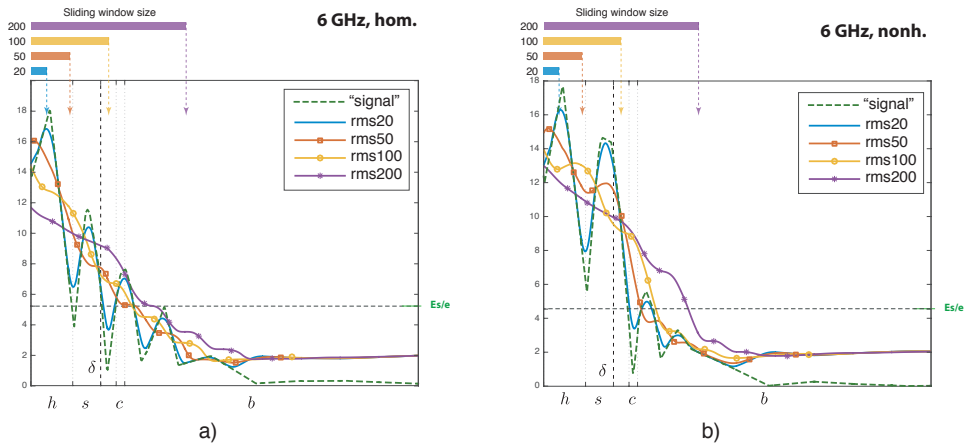


Fig. 11. Incident EM wave frequency  $f=6$  GHz. Envelope of signal (electric field distribution) on the horizontal axis of a) homogeneous and b) non-homogeneous spherical models. Envelope obtained using an RMS approach with sliding window size of 20, 50, 100, and 200 points.  $X$ -axis denotes model tissue (compartment):  $h$  - head,  $s$  - skull,  $c$  - CSF,  $b$  - brain; points separation is  $90 \mu\text{m}$ .  $\delta$  is penetration depth at particular frequency.  $E_s/e$  denotes the 37% value of electric field at the surface.

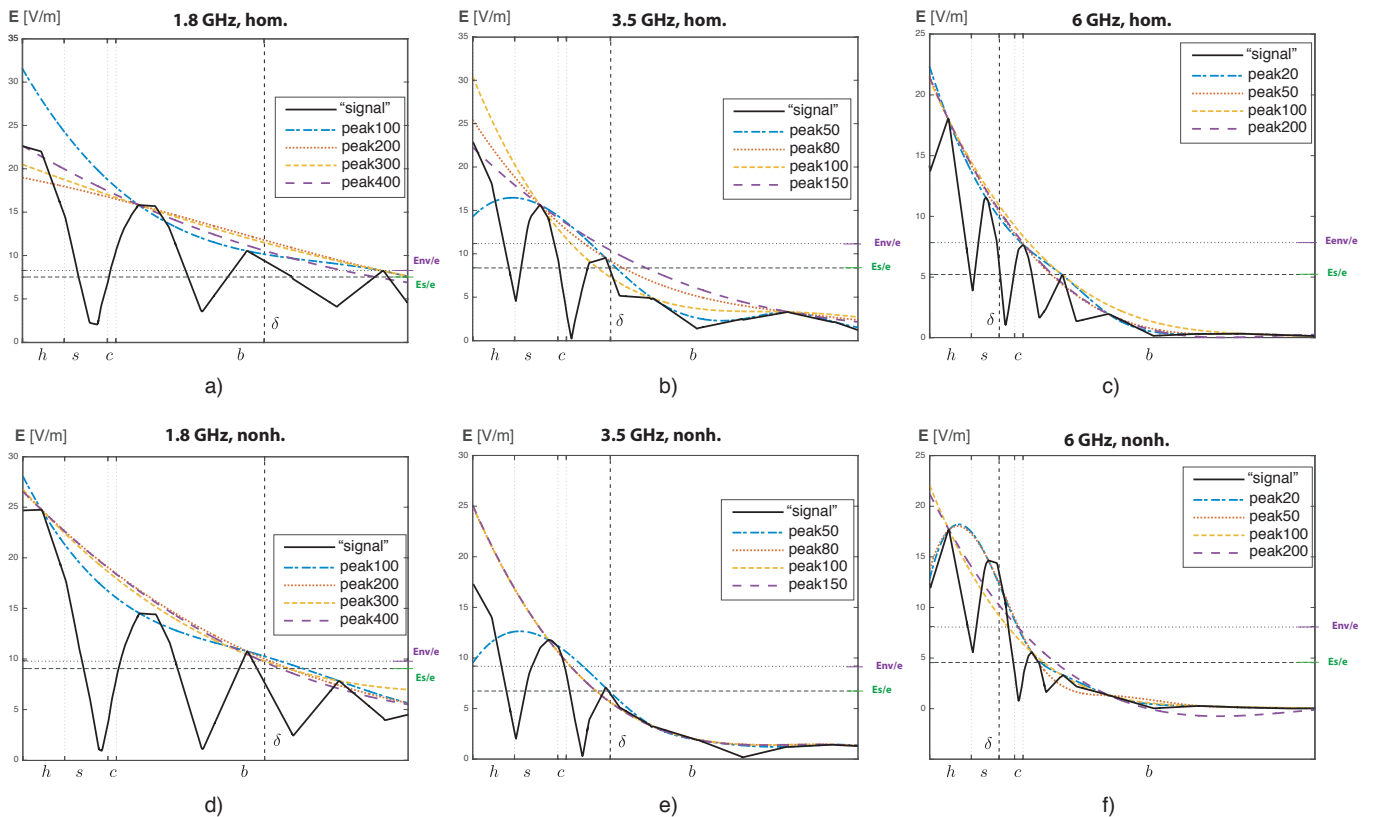


Fig. 12. Envelope of electric field distribution at several frequencies of incident EM wave (1.8 GHz, 3.5 GHz, 6 GHz) along horizontal axis of homogeneous (a-c) and non-homogeneous (d-f) spherical head models. Envelope obtained using  $N$ -points separations between the local maxima (peak  $N$ ).  $X$ -axis denotes model tissue (compartment):  $h$  - head,  $s$  - skull,  $c$  - CSF,  $b$  - brain; points separation is  $90 \mu\text{m}$ .  $\delta$  is penetration depth at particular frequency.  $E_{nv}/e$  and  $E_s/e$  denote the 37% value of envelope and electric field at the surface, respectively.

after some rearranging, the following expression for the wavelength is obtained:

$$\lambda = \frac{\lambda_0}{\sqrt{\frac{\varepsilon_r}{2} \left[ 1 + \sqrt{1 + \frac{\sigma^2}{\omega^2 \varepsilon_0^2 \varepsilon_r^2}} \right]}} \quad (23)$$

Finally, the penetration depth  $\delta$  can be found as follows. Inserting (22) into (21):

$$\frac{1}{\lambda^2} = \frac{\omega^2 \varepsilon_r}{8\pi^2 c^2} \left[ 1 + \sqrt{1 + \frac{\sigma^2}{\omega^2 \varepsilon_0^2 \varepsilon_r^2}} \right] \quad (24)$$

and after some additional work, results in the expression for penetration depth:

$$\delta = \frac{c}{\omega \sqrt{\frac{\varepsilon_r}{2} \left[ \sqrt{1 + \frac{\sigma^2}{\omega^2 \varepsilon_0^2 \varepsilon_r^2}} - 1 \right]}} \quad (25)$$

In case of a good conductor, or if the following is satisfied:

$$\sigma \gg \omega \varepsilon_0 \varepsilon_r \quad (26)$$

the well known expressions for  $\delta$  and  $\lambda$  are obtained:

$$\delta \approx \sqrt{\frac{2}{\omega \mu_0 \sigma}} \quad (27)$$

$$\lambda \approx \frac{2\pi}{\sqrt{\pi f \sigma \mu_0}} \approx 2\pi\delta \quad (28)$$

## REFERENCES

- [1] D. Poljak and M. Cvetković, *Human Interaction with Electromagnetic Fields: Computational Models in Dosimetry*. Academic Press, 2019.
- [2] A. Hirata, Y. Diao, T. Onishi, K. Sasaki, S. Ahn, D. Colombi, V. De Santis, I. Laakso, L. Giaccone, W. Joseph et al., "Assessment of human exposure to electromagnetic fields: Review and future directions," *IEEE Transactions on Electromagnetic Compatibility*, vol. 63, no. 5, pp. 1619–1630, 2021.
- [3] IEEE, "IEEE Standard for safety levels with respect to human exposure to electric, magnetic, and electromagnetic fields, 0 Hz to 300 GHz," *IEEE Std C95.1-2019*, pp. 1–312, 2019.
- [4] ICNIRP, "Guidelines for limiting exposure to electromagnetic fields (100 kHz to 300 GHz)," *Health Physics*, vol. 118, no. 5, pp. 483–524, 2020.
- [5] S. Kodera, J. Gomez-Tames, and A. Hirata, "Temperature elevation in the human brain and skin with thermoregulation during exposure to RF energy," *Biomedical engineering online*, vol. 17, no. 1, pp. 1–17, 2018.
- [6] K. R. Foster, M. C. Ziskin, Q. Balzano, and G. Bit-Babik, "Modeling tissue heating from exposure to radiofrequency energy and relevance of tissue heating to exposure limits: Heating factor," *Health Physics*, vol. 115, no. 2, pp. 295–307, 2018.
- [7] P. Wainwright, "Computational modelling of temperature rises in the eye in the near field of radiofrequency sources at 380, 900 and 1800 MHz," *Physics in Medicine & Biology*, vol. 52, no. 12, p. 3335, 2007.
- [8] A. Šušnjara, H. Dodig, D. Poljak, and M. Cvetković, "Stochastic-deterministic thermal dosimetry below 6 GHz for 5G mobile communication systems," *IEEE Transactions on Electromagnetic Compatibility*, vol. 63, no. 5, pp. 1667–1679, 2021.
- [9] M. C. Ziskin, S. I. Alekseev, K. R. Foster, and Q. Balzano, "Tissue models for RF exposure evaluation at frequencies above 6 GHz," *Bioelectromagnetics*, vol. 39, no. 3, pp. 173–189, 2018.
- [10] K. Li, K. Sasaki, S. Watanabe, and H. Shirai, "Relationship between power density and surface temperature elevation for human skin exposure to electromagnetic waves with oblique incidence angle from 6 GHz to 1 THz," *Phys. Med. Biol.*, vol. 64, no. 6, p. 065016, 2019.
- [11] K. Li, S. Kodera, D. Poljak, Y. Diao, K. Sasaki, A. Šušnjara, A. Prokop, K. Taguchi, J. Xi, S. Zhang et al., "Calculated epithelial/absorbed power density for exposure from antennas at 10–90 GHz: Intercomparison study using a planar skin model," *IEEE Access*, vol. 11, pp. 7420–7435, 2023.
- [12] D. Poljak, A. Šušnjara, and A. Fišić, "Assessment of transmitted power density in the planar multilayer tissue model due to radiation from dipole antenna," *Journal of Communications Software and Systems*, vol. 19, no. 1, pp. 39–51, 3 2023. [Online]. Available: <https://doi.org/10.24138/jcomss-2022-0050>
- [13] K. Li, T. Hikage, H. Masuda, E. Ijima, A. Nagai, and K. Taguchi, "Parameter variation effects on millimeter wave dosimetry based on precise skin thickness in real rats," *Scientific Reports*, vol. 13, no. 1, p. 17397, 2023.
- [14] M. Cvetković, A. Lojić Kapetanović, D. Poljak, and H. Dodig, "On the applicability of numerical quadrature for double surface integrals at 5G frequencies," *Journal of Communications Software and Systems*, vol. 18, no. 1, pp. 42–53, 2022.
- [15] R. Novak, "Viability of numerical full-wave techniques in telecommunication channel modelling," *Journal of Communications Software and Systems*, vol. 16, no. 4, pp. 269–278, 10 2020. [Online]. Available: <https://doi.org/10.24138/jcomss.v16i4.1041>
- [16] M. Cvetković, D. Poljak, and H. Dodig, "Numerical filtering of electric field in human head models exposed to high-frequency emf," in *2023 International Conference on Software, Telecommunications and Computer Networks (SoftCOM)*, 2023, pp. 1–6.
- [17] H. Dodig, D. Poljak, and M. Cvetković, "On the edge element boundary element method/finite element method coupling for time harmonic electromagnetic scattering problems," *International Journal for Numerical Methods in Engineering*, vol. 122, no. 14, pp. 3613–3652, 2021.
- [18] M. He, J. Liu, B. Wang, C. Zhang, and H. Sun, "On the use of continuity condition in the fast solution of volume-surface integral equation," *IEEE Antennas and Wireless Propagation Letters*, vol. 16, pp. 625–628, 2016.
- [19] C. Gabriel, "Compilation of the dielectric properties of body tissues at RF and microwave frequencies," Brooks Air Force Base, TX. Report: AL/OE-TR-1996-0037, Tech. Rep., 1996.
- [20] Y. Ji, X. Meng, J. Shao, Y. Wu, and Q. Wu, "The generalized skin depth for polarized porous media based on the cole-cole model," *Applied Sciences*, vol. 10, no. 4, p. 1456, 2020.
- [21] S. Qiu, B. Ma, Q. Wu, R. Qu, B. Shi, H. Luan, and Y. Ji, "Numerical calculation of diffusion depth and skin depth based on a gemtip model in electromagnetic sounding methods," *IEEE Transactions on Geoscience and Remote Sensing*, vol. 60, pp. 1–9, 2022.
- [22] N. P. Singh and T. Mogi, "Effective skin depth of em fields due to large circular loop and electric dipole sources," *Earth, planets and space*, vol. 55, no. 6, pp. 301–313, 2003.
- [23] D. Rice, V. Venkatachalam, and M. Wegmann, "A simple envelope detector," *IEEE Transactions on Instrumentation Measurement*, vol. 37, no. 2, pp. 223–226, 1988.
- [24] Y. Yang, "A signal theoretic approach for envelope analysis of real-valued signals," *IEEE Access*, vol. 5, pp. 5623–5630, 2017.



**Mario Cvetković** received his B.Sc. degree in electrical engineering from the University of Split, Croatia, in 2005. In 2009 he obtained M.Phil. degree in engineering and electrical engineering from the Wessex Institute of Technology, University of Wales, Cardiff, U.K. In 2013 he received his Ph.D. degree in engineering and electrical engineering from the University of Split, in 2013. He is currently an Associate Professor with the Faculty of Electrical Engineering, Mechanical Engineering, and Naval Architecture (FESB), University of Split, where he teaches the fundamentals of the electrical engineering course. He has authored or coauthored 90 papers in international journals, conference proceedings, and several book chapters. In 2019, he coauthored a book entitled *Human Interaction with Electromagnetic Fields - Computational Models in Dosimetry* (St. Louis, MO, USA: Elsevier, 2009). His research interests include numerical modeling with finite elements and method of moments, computational bioelectromagnetics, and heat transfer related phenomena. He is a Member of the International Committee on Electromagnetic Safety (ICES) Technical Committee 95. He was the recipient of the Best Student Paper Award, awarded at the 16th Edition of the International Conference SoftCOM 2008.



**Hrvoje Dodig** (M'18) received a B.Sc. EE degree from the Faculty of Electrical Engineering, Mechanical Engineering and Naval Architecture (FESB) at the University of Split, Croatia in 2002. He was awarded the Chevening scholarship grant for post-graduate study in computational electromagnetics at the Wessex Institute of Technology, UK and received a M.Sc. EE degree from both the Wessex Institute of Technology, UK and the Faculty of Electrical Engineering, Mechanical Engineering and Naval Architecture (FESB) at the University of Split, Croatia in 2005. He received his Ph.D. EE degree from the Wessex Institute of Technology, UK in 2012. From 2013 to 2016 he was with the Department of Radar Technology at the Naval Electronic Center, Croatia, and he was the head of hardware and software design of military communication equipment. Since 2016 he is lecturer at the Department of Naval Electronic and Information Technology at University of Split (PFST). He became assistant professor in 2018 and he teaches electronic circuits, robotics, software design, and algorithms. From 2018-2021 was vice dean of research and became associate professor in 2023. His research interests include numerical modeling of electromagnetic fields, boundary and finite element methods, hybrid numerical methods, electromagnetic compatibility, electromagnetic scattering problems and the development of general electromagnetic theory.



**Dragan Poljak** (SM' 13) received his PhD in el. Eng. in 1996 from the Univ. of Split, Croatia. He is the Full Prof. at Dept. of Electron. and Computing, Univ. of Split. His research interests are oriented to computational electromagnetics (electromagn. compatibility, bioelectromagnetics and plasma physics). To date Prof. Poljak has published more than 160 journ. and 250 conf. papers, and authored some books, e.g. two by Wiley, New Jersey and one by Elsevier, St Louis. He is a Senior member of IEEE, a member of Editorial Board of Eng. Anal. with Boundary Elements, Math. Problems in Eng. And IET Sci. Measur. & Techn. He was awarded by several prizes for his achievements, such as National Prize for Science (2004), (2023) Croatian sect. of IEEE annual Award (2016), Technical Achievement Award of the IEEE EMC Society (2019) and George Green Medal from University of Mississippi (2021). From May 2013 to June 2021 Prof. Poljak was a member of the board of the Croatian Science Foundation. He is currently involved in ITER physics EUROfusion collab. and in Croatian center for excellence in research for tech. sciences. He is active in few Working Groups of IEEE/Internat. Committee on Electromagnetic Safety (ICES) Tech. Comm. 95 SC6 EMF Dosimetry Modeling.